Synthesis and characterisation of sodium silicate from spent foundry sand: Effective route for waste utilisation

Abdul Aleem Mohamed Ismail, Kavikumaran Kannadasan, Prabunathan Pichaimani, Hariharan Arumugam, Alagar Muthukaruppan[*]

Polymer Engineering Laboratory, Department of Civil Engineering, PSG Institute of Technology and Applied Research, Neelambur, Coimbatore, 641 062, Tamilnadu, India

A B S T R A C T

In this study, spent foundry sand (SFS) was treated and used as a source to synthesis sodium silicate. Initially, SFS was subjected to calcination (C-SFS) followed by acid bleaching (A-SFS) to yield quartz silicate in high purity. After each treatment, the samples were studied using field emission scanning electron microscopy (FE-SEM) and X-ray diffraction (XRD) to analyse their properties. The hydrothermal process was performed using A-SFS with alkali hydroxides to obtain the corresponding alkali silicates. The optimisation studies conducted at different temperatures and time periods revealed that the maximum yield of 97.6% was obtained at 225 °C for 3 h. A plausible depolymerisation mechanism is also proposed based on the observations from ^{29}Si NMR and XRD results of residues. Thus, present study facilitates the synthesis of sodium silicate effectively by utilising SFS, which in turn minimizes the waste disposal.

© 2020 Elsevier Ltd. All rights reserved.

1. Introduction

Metal casting industries routinely use moulds composed of quartz sand (Siddique et al., 2018). After repeated castings, the moulds become unusable and are discarded as Spent foundry sand (SFS) in large quantities (Arulrajah et al., 2017). The American Foundry Society has reported that typically, about 1 t of quartz sand is required for each ton of iron or steel cast produced (US DOT, 1998). Consequently, about 100 Mt of consumed sand is discarded annually worldwide as SFS (Díaz Pace et al., 2017). Based on its origin, SFS is classified into two types: i) green sand (GS), which is moulded using bentonite clay, bituminous coal, and water and ii) core sand (CS), which is composed of silica moulded with either organic resin or sodium silicate binders (Torres et al., 2017). Owing to the presence of heavy metals in the fractional quantity and phenolic organic pollutants, hazardous elements and compounds can leach from both types of sand, which can cause severe environmental pollution in landfills (Siddiquea et al., 2010).

Several researchers have investigated the bulk reutilization of SFS in civil and geotechnical engineering applications (Basar and DeveciAksoy, 2012). SFS have been used as partial replacement of aggregate in asphalt concrete (Bakis et al., 2006), highway sub-bases (Guney et al., 2006), highway embankment construction (Partridge et al., 1999), flowable fill (Bhat and Lovell, 1997), clay bricks (Alonso-Santurde et al., 2011), hydraulic barriers (Tarek et al., 2000), and concrete (Khatib and Ellis, 2001). Nevertheless, tons of SFS are deserted all over the world; therefore, an investigation that provides value addition to SFS is still highly desirable, which will minimise its adverse environment effects. Recently, Souza et al., (2019) reported the production of plasma electrolytic oxidation ceramic coating usingSFS. Xiang et al. (2019) explored the possibilities of SFS in refractory industries from the crystalline and microstructure studies at different thermal conditions (1300−1500 °C).

Sodium silicate, also known as water glass, is composed of silicates acts as either binders or formulation additives in various industries (Alam et al., 2019). In 2017, the sodium silicate market value was estimated to be USD 8.8 × 10^9 and is expected to reach USD 11.7 × 10^9 by 2024 (Zion Market Research, 2019). The sodium silicate market is driven by the rising demands for detergents, precipitated silica, adhesives, sealants, construction, pulp and paper, water treatment, metal casting, and food preservation (Van Dokkum et al., 2004). Conventionally, the reaction of silica sand

with soda ash at elevated temperatures of 1000−1400 °C forms water glass, which is crushed and digested with steam under pressure to obtain sodium silicate of the desired density (Friedman, 1948). Laudise and Ballman (1961) studied the effective depolymerisation of quartz in alkali, which also led to the formation of alkali silicate without need of high temperature. Anderson and Burnham (1965) have reported the solubility of quartz in supercritical aqueous solutions. Meanwhile, it is important to note that the main crystalline phase of SFS was observed to be quartz (de Matos et al., 2019). Synthesis of sodium silicate using SFS could impart benefits like waste utilisation, minimise the rate of quartz depletion and reduce environmental issues. Thus far, no significant research has been devoted to the production of sodium silicate from SFS.

In the present work sodium silicate is synthesized from SFS through a hydrothermal approach. The optimum conditions with regard to the reaction temperature and reaction time have been extensively studied. The synthesis proceeds through depolymerisation of the quartz by alkaline hydrolysis. The depolymerisation mechanism is proposed based on the observed results of FE-SEM, XRD, and ^{29}Si NMR analysis, which are all discussed and reported in detail.

2. Materials and methods

2.1. Materials

SFS was collected from a local foundry (PSG Foundry Division, Neelambur, Coimbatore, 641062, India), and laboratory grade (LR) NaOH and HCl were purchased from SRL, India. The physical properties such as appearance, specific gravity, bulk density, and grain size distribution are presented in Table 1.

2.2. Preliminary treatment of SFS

The phenolic carbon, pulverised coal, and metal impurities, resulting in black colour of the SFS (Table 1), were removed prior to the hydrothermal process. Initially, the SFS was subjected to calcination at 500 °C for 2 h, and it appears dark brown in colour (Table 1). This is referred to as C-SFS. After cooling to room temperature, the C-SFS was refluxed using 1 M HCl under constant stirring for 5 h. The sample was then neutralised by repeated rinsing with water and was dried at 90 °C for 3 h. The dried sample obtained, referred to as A-SFS appears light brown in colour (Table 1) and was preserved until further experimentation.

2.3. Synthesis of sodium silicate

The A-SFS sample obtained after preliminary treatment was made to react with 2 equivalents of NaOH under hydrothermal condition. In this context, 10 g (0.166 mol) of A-SFS and 13.2 g (0.33 mol) of NaOH were mixed with 25 mL of water and were transferred into a Teflon-lined pressure vessel. The pressure vessel was subjected to varying temperatures ranging from 150 °C to 250 °C for different periods from 1.5 h to 12 h. The residues collected after each process were separated and weighed to calculate the percentage yield of sodium silicate. The collected silica residues are represented as $R_{x/y}$, where R = residue (%), x = time (h), and y = temperature (°C). The yield of sodium silicate was calculated using equation (1):

$$Yield\ (\%) = 100 \\ - \left[\frac{Weight\ of\ residue\ obtained\ after\ hydrothermal\ process}{Weight\ of\ A-SFS}\right] X\ 100$$
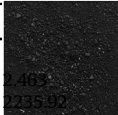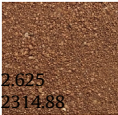
(1)

2.4. Analysis methods

The diffraction patterns were recorded using PAN analytical X'pert3 powder (PANalytical, Eindhoven, The Netherlands) in the 2θ range of 10−80°. Elemental compositions were analysed using Bruker S8 Tiger X-Ray Fluorescence spectrometer (XRF; Bruker, Germany). The surface morphologies and elemental profiles of the pre-treated samples and residues were examined using Field Emission Scanning Electron Microscopy (FE-SEM; Gemini 0336, Zeiss Sigma, San Diego, California, USA) including Energy Dispersive X-ray Spectrometry (EDS; XFlash, Bruker, Germany). The residual analyses of the A-SFS were analysed using the solid state ^{29}Si nucleus in a Fourier Transform (FT)-NMR spectrometer (AVANCE III HD-500 MHz, Bruker, Germany). The synthesized sodium silicate was analysed by using an NMR spectrometer (AVANCE III 500 MHz (Bruker, Germany) using D$_2$O as solvent.

3. Results and discussion

3.1. Treated SFS

Before converting SFS into sodium silicate, a detailed study was conducted on the feed sand (virgin sand) in comparison with SFS to identify the crystalline arrangement and morphological nature. These data are essential parameters in proposing the mechanism involved in the preparation of sodium silicate using SFS. The feed sand appears in pale yellow colour (Table 1) and has a bulk density of 2431.54 kg/m^3. Fig. 1 presents the XRD patterns of both the feed and SFS along with treated C-SFS and A-SFS samples. Strong intense peaks observed at 2θ = 21.0° and 26.7° corresponded to the (100) and (101) planes of the silicate network representing low quartz crystals with hexagonal structures and the $P3_121$ space group. The

Table 1
Physical properties of feed sand, SFS, C-SFS, and A-SFS.

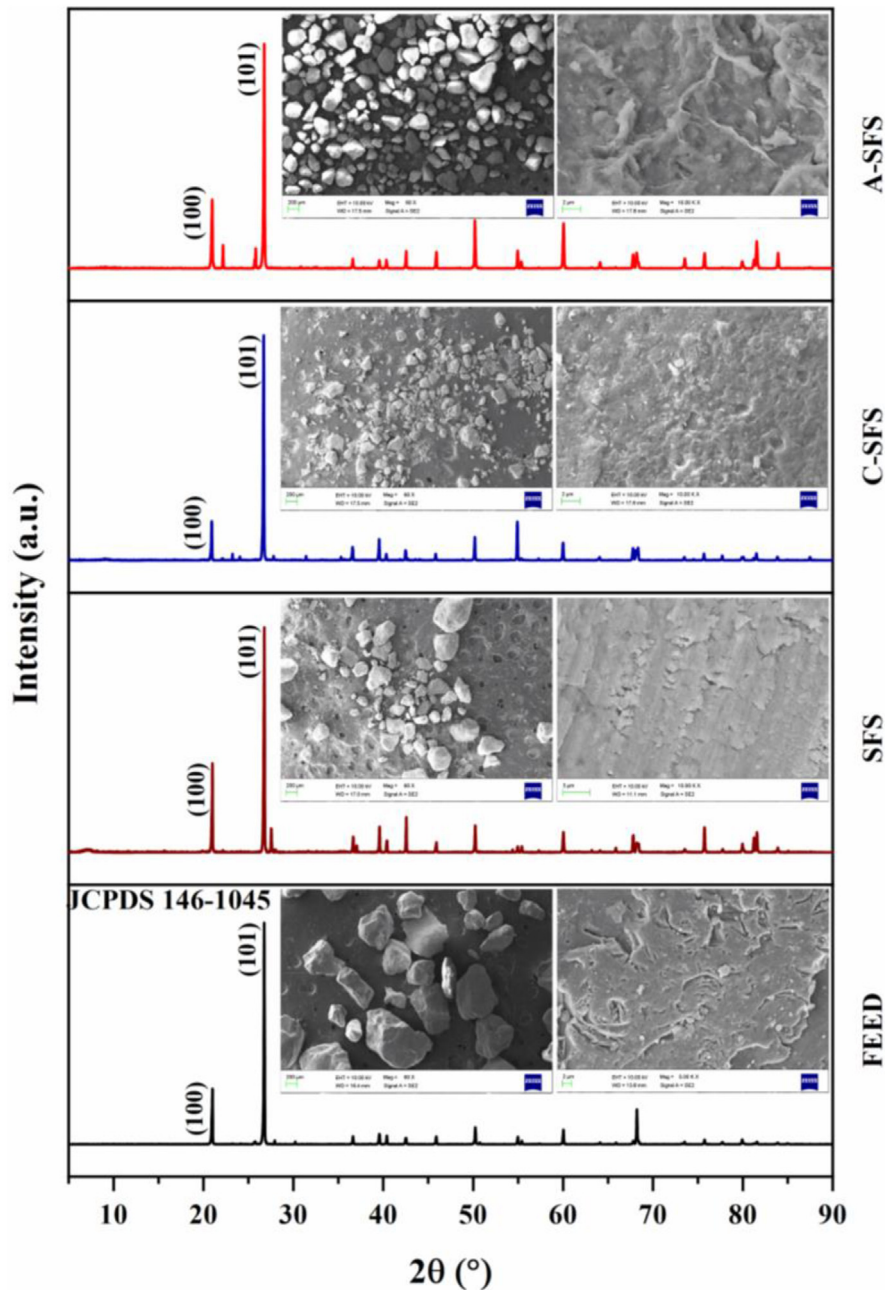| Description					
Appearance					
Specific gravity		2.660	2.465	2.625	2.487
Bulk density (kg/m^3)		2431.54	2235.92	2314.88	2357.25
Grain size distribution (*Retained percentage* (%))	2.36 mm	0	0	0	0
	1.18 mm	0.60	1.02	0.67	0.74
	600 μm	5.68	9.60	10.53	9.06
	425 μm	14.22	17.26	19.70	13.74
	300 μm	23.49	27.84	28.43	24.02
	150 μm	52.38	40.90	37.70	47.49
	90 μm	2.95	2.63	2.20	4.41
	75 μm	0.69	0.74	0.73	0.54

Fig. 1. XRD patterns of feed sand, SFS, C-SFS, and A-SFS, with SEM images shown in the inset.

obtained diffraction patterns are in accordance with that of JCPDS 146−1045 (Mastella et al., 2014). It is interesting to note that the primary treatments (calcination and acid bleach) did not alter the crystalline nature of the sand as evidenced from the similar XRD pattern presented in Fig. 1. In spite of their similar crystal structures, the appearance of SFS, C-SFS, and A-SFS are observed to be different. Black colour of SFS is due to the presence of carbon powders added during the moulding process (Table 1). In addition, the bulk density of SFS was observed to be 2235.92 kg/m^3. To quantify the percentage of carbon in SFS, EDS analysis was carried out and presented in Fig. S1. The EDS profile of SFS shows the presence of carbon (28.8%), aluminium (1.08%), and traces of metal oxides in addition to silica.

The micrograph images obtained from the FE-SEM analysis is presented in the inset of Fig. 1. Both the feed sand and SFS samples

showed individual grains with different shapes including rounded to sub-rounded and angular to sub-angular and a wide range of sizes. The morphologies of the feed sand presented in the inset of Fig. 1 exhibit V-shaped patterns with straight and curved scratches at higher magnification. These morphologies are typical features of sand obtained from marine environments (Raza et al., 2018). The morphologies of SFS show no curved scratches or patterns (Fig. 1). This phenomenon is due to the densification of silicate grains subjected to high-temperature during casting process. The fused silicates with closely packed morphologies were observed at higher magnification.

It is also highly beneficial to compare the morphologies of the sand and treated samples. The SEM images provided in the inset of Fig. 1 show no significant changes in morphology after the calcination process, whereas samples subjected to acid bleaching

showed rough surfaces. The element mapping and elemental composition of C-SFS and A-SFS samples are presented in Fig. S2 and Fig. S3 respectively. After calcination, the SFS changes to dark brown colour (C-SFS) and has bulk density of 2314.88 kg/m^3. This phenomenon accounts for the removal of carbon during the calcination process (de Matos et al., 2020)and accordingly no carbon signal was observed in the EDS profile (Fig. S2). The appearance of dark brown colour of C-SFS is due to the presence of dead bentonite clay and metal oxides, which is evidenced from EDS profile and elemental mapping (Fig. S2). However, due to dissolution of bentonite clay and metal oxides during acid bleach the brown colour turns into light brown with increased bulk density value (2357.25 kg/m^3). In order to validate the dissolution of clay and metal oxides, XRF analysis was also performed in addition to EDS profile (Fig. S3). The XRF elemental compositions of C-SFS and A-SFS are presented in Table S1. It is observed that the percentage of metal oxides present in A-SFS are lower than those of C-SFS, which accounts for the dissolution and removal (Balbay, 2019).

The solid state ^{29}Si NMR spectra of the feed sand, SFS, C-SFS, and A-SFS samples are presented in Fig. 2. The feed sand showed an intense, sharp peak at −107.5 ppm, which corresponds to the Q^4(SiO$_4$) network of the three-dimensional siloxane frameworks of quartz polymorphs of silica (Anbalagan et al., 2010). This result supports the quartz peaks of the feed sand presented in the diffractogram pattern of Fig. 1. In case of SFS, two weak ^{29}Si signals were observed, which were attributed to the Q^4 siloxane and Q^3 silanol networks (Allu et al., 2018). The presence of residual carbon impedes the silicon signals and thereby increases the signal-to-noise ratio. Post calcination, the C-SFS showed more peaks between −92.5 ppm and −114.5 ppm as well as a major signal at −107.5 ppm. This result might be attributed to the formation of silanol and amorphous quartz corresponding to the Q^3 and Q^4 signals respectively (Wijnen et al., 1989). Interestingly, the acid-treated sample (A-SFS) showed a single strong signal at −107.5 ppm, which implies the existence of a Q^4 siloxane network and the removal of silanol groups along with other acid-soluble impurities. The preliminary treatment of SFS yielded pure quartz phase silica, which was used for the synthesis of sodium silicate as a value-added product.

3.2. Synthesis of sodium silicate

The synthesis of sodium silicate was conducted by using 10 g of A-SFS possessing silica of low-quartz and 2 mol equivalents of NaOH at 200 °C for 12 h in a closed pressure vessel. After cooling to room temperature, the viscous solution, with a density of 1.48 g/m^3, was collected and subjected to ^{29}Si NMR analysis. Fig. 3 shows the ^{29}Si NMR spectrum of sodium silicate, in which the appearance of intense chemical shifts δ at −71.4, −79.4, and −81.5 ppm correspond to the silicic acid monomer (Q^0 = tetrahedral unit of SiO$_4$), dimer (Q$^1_2$), and cyclic trimer (Q$^2_3$) respectively. Owing to the presence of the cyclic tetramer (Q$^2_4$) and the prismatic hexamer (Q$^3_6$), weak signals were observed at chemical shifts δ occurring at −87.7 and −89.6 ppm respectively in Fig. 3, which are in accordance with reported literature (Bass and Turner, 2002). This confirms the occurrence of depolymerisation of three-dimensional siloxane frameworks of quartz polymorphs into disconnected SiO$_4^{4-}$ tetrahedral units, pyrosilicate tetrahedral SiO$_4^{4-}$ and cyclic trisilicate combining three SiO$_4^{4-}$ tetrahedralunits (Moravetski et al., 2002). This result validates the formation of sodium silicate using the hydrothermal method. Due to the effective intercalation of the Na$^+$ and OH$^-$ ions in the low-quartz crystal lattices during the high temperature exposure under pressure (hydrothermal process), depolymerisation of the quartz network occurred, which caused the silicate species to become suspended in a viscous solution (Fig. 3). The mechanism of depolymerisation is discussed based on the results of the residues analysed. Also, optimisation studies were conducted using various reaction time periods, reaction temperatures and with KOH.

3.3. Depolymerisation mechanism

To evaluate the possible depolymerisation mechanism, the silica residues obtained after different reaction time periods were subjected to ^{29}Si NMR analysis. The ^{29}Si NMR spectra of the residues collected after 3, 6, and 9 h are presented in Fig. 4 along with their silicate functionality. Because the residue collected after 12 h was insignificant in quantity, its NMR results were excluded. As previously discussed, the signal at −107.4 ppm (Fig. 2), corresponding to the Q^4 (SiO$_4$) quartz polymorphs (Anbalagan et al., 2010) began to
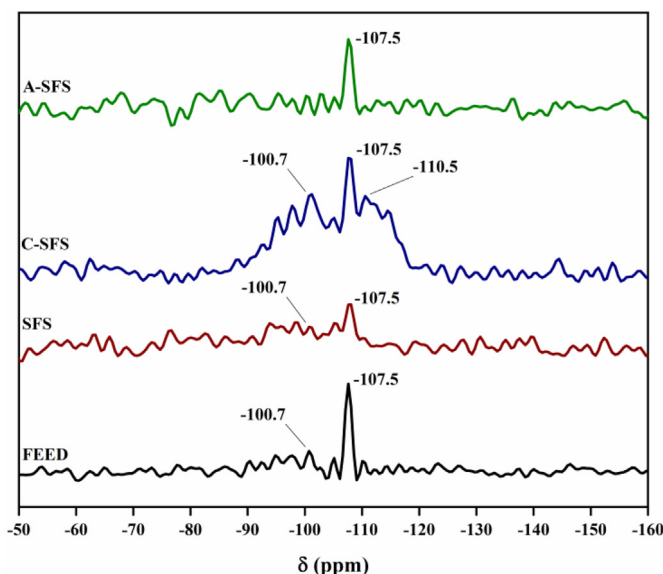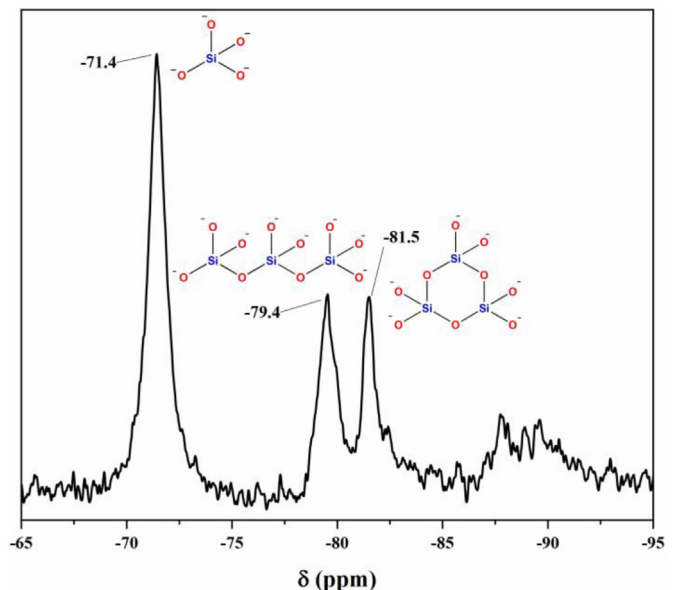
Fig. 2. ^{29}Si NMR of feed sand, SFS, C-SFS, and A-SFS samples.

Fig. 3. ^{29}Si NMR results of prepared sodium silicate.

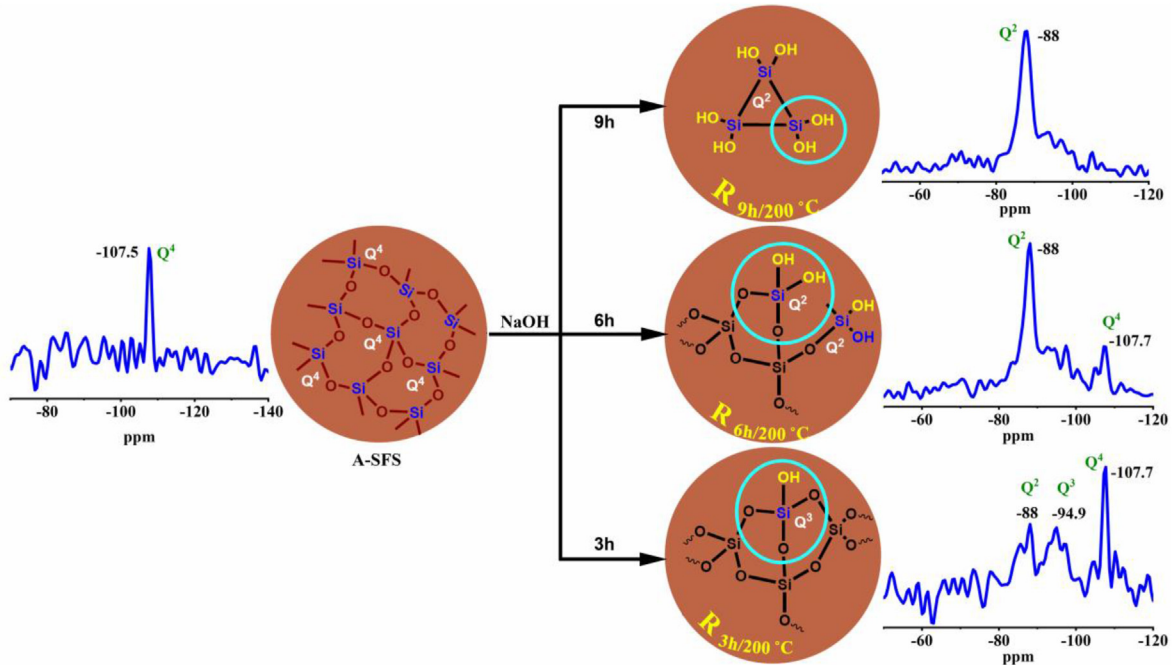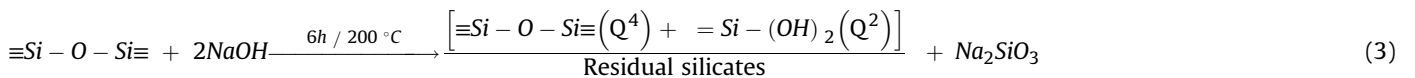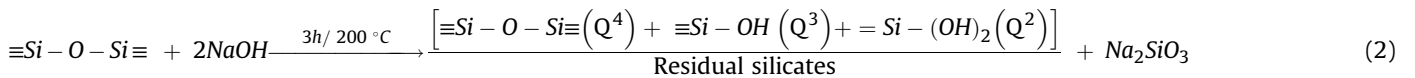**Fig. 4.** ^{29}Si NMR spectra of silica residues obtained after 3, 6, and 9 h.
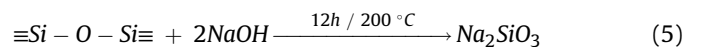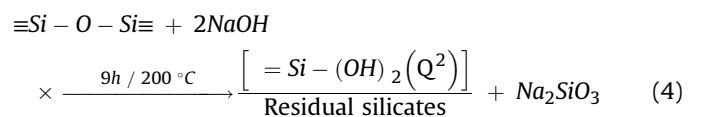
disappear as the time of hydrothermal subjection increased. This behaviour is clearly demonstrated in the ^{29}Si NMR spectra of the residues presented in Fig. 4. On the basis of this spectral evidence, the depolymerisation mechanism with respect to time period is proposed in equations (2)–(5). The residues ($R_{3h/200\,°C}$) collected after 3 h tends to show the appearance of new signals at -88.0 and -94.9 ppm in addition to -107.4 ppm signal (Fig. 4), which correspond to the chemical shift values of the Q^2, Q^3, and Q^4 silicates and the siloxane signals respectively (equation (2)). The hydration

present in trace amounts (equation (3)). The chemical shift observed at -88 ppm became appreciably intense after 9 h, which suggests the presence of a completely depolymerised silicate network belonging to Q^2 functionality with no Q^4 signal (equation (4)) (Khouchaf et al., 2009). The sodium silicate collected after 12 h (equation (5)) shows chemical shifts δ at -71.4, -79.4, and -81.5 ppm corresponding to the silicic acid monomer (Q^0 = tetrahedral unit of SiO_4), dimer (Q^1_2), and cyclic trimer (Q^2_3), respectively as presented in Fig. 3 (Pfeiffer et al., 2019).

$$\equiv Si - O - Si \equiv \ + \ 2NaOH \xrightarrow{3h/\ 200\ °C} \underbrace{\left[\equiv Si - O - Si \equiv \left(Q^4 \right) + \ \equiv Si - OH \left(Q^3 \right) + = Si - (OH)_2 \left(Q^2 \right) \right]}_{\text{Residual silicates}} \ + \ Na_2SiO_3 \tag{2}$$

$$\equiv Si - O - Si \equiv \ + \ 2NaOH \xrightarrow{6h\ /\ 200\ °C} \underbrace{\left[\equiv Si - O - Si \equiv \left(Q^4 \right) + \ = Si - (OH)_2 \left(Q^2 \right) \right]}_{\text{Residual silicates}} \ + \ Na_2SiO_3 \tag{3}$$

of quartz silicate under hydrothermal condition begins with the formation of Q^2 and Q^3 silanols initially, as presented in equation (2). For the synthesis of sodium silicate from quartz, an essential step is the initiation of the depolymerisation process influenced by the OH^- ion as a nucleophile. This process proceeds with the breaking of a siloxane bond ($\equiv Si-O-Si \equiv$) through nucleophilic attack of alkali, which cleaves the Q^4 into silanol (Q^3, Q^2, and Q^1) networks (Gratz et al., 1990).

As the time period of hydrothermal subjection increases, the depolymerisation is promoted through the formation of Q^2 and Q^1 silanols (equations (3)–(5)) silicates. The residues collected after 6 h and 9 h showed an intense signal of Q^2 silicate moieties at δ -88 ppm (Smith et al., 1983). The residue collected after 6 h showed a weak signal corresponding to the Q^4 silicate region, which indicates that three-dimensional silicate of quartz was

$$\equiv Si - O - Si \equiv \ + \ 2NaOH$$

$$\times \xrightarrow{9h\ /\ 200\ °C} \underbrace{\left[= Si - (OH)_2 \left(Q^2 \right) \right]}_{\text{Residual silicates}} \ + \ Na_2SiO_3 \tag{4}$$

$$\equiv Si - O - Si \equiv \ + \ 2NaOH \xrightarrow{12h\ /\ 200\ °C} Na_2SiO_3 \tag{5}$$
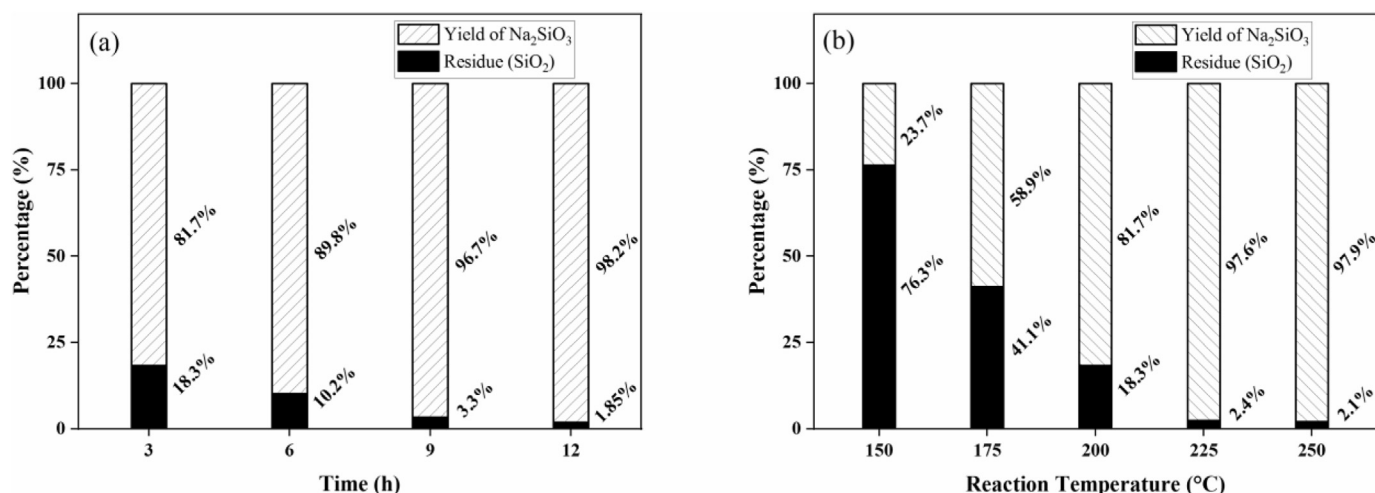
Fig. 5. Yield and residual analysis at (a) 200 °C at different time periods and (b) temperatures for 3 h.

3.4. Optimisation studies

3.4.1. Optimisation of time

The sodium silicate collected after 12 h of subjection in a closed vessel with 2 mol equivalents of NaOH amounted to about 98.2%. Further optimisation was conducted with respect to different time periods of 3, 6, and 9 h keeping a constant temperature of 200 °C. The yields of sodium silicate obtained in the different time periods are presented in Fig. 5(a). It is interesting to note that 81.7% yield was achieved after subjection of 3 h. The left over silica residue requires an additional 9 h for complete depolymerisation. Thus, 12 h of subjection afforded 98.2% as the maximum yield. Further, an experiment was performed for 1.5 h at 200 °C to observe the formation yield. Only 43% yield was observed, suggesting that minimum 3 h subjection is required to achieve high yield. In addition, the residues collected after each period were analysed to validate the depolymerisation of the low quartz of A-SFS.

Fig. 6 presents the micrographs of low-quartz residues obtained from FE-SEM at different time periods of 3, 6, and 9 h keeping a constant temperature of 200 °C. The low quartz of the A-SFS sample tended to exhibit disintegrated grain structures, which was verified by the residual results of the micrograph analysis. The sample subjected to 3 h showed a densely packed hexagonal array of the low-quartz silicate network. However, the sample subjected to 6 h tended to show free hexagonal rods with a micro-granular appearance. The residue collected after 9 h showed only micro-granular morphology. XRD analysis was also performed on the residues, as shown in Fig. 6. The diffractions of the collected silica residues showed different patterns. The residue obtained after 3 h showed major peaks at $2\theta = 20.9°$ and $26.7°$ corresponding to the (001) and (101) planes of quartz, respectively (JCPDS: 146−1045). The diffraction patterns for the residue obtained after 3 h showed patterns similar to those of A-SFS, which indicates the residues belong to the hexagonal crystal form with the $P3_121$ space group of low quartz. The intensities of the peaks were significantly lower, which might be attributed to the depolymerisation of the silicates. The results obtained from the analysis of the residues of samples collected after 6 h and 9 h showed interesting features. The major peak at $2\theta = 26.7°$ corresponding to the (101) plane disintegrated into four minor peaks, which implies effective depolymerisation of the quartz silica with NaOH. It is concluded that the effective completion of depolymerisation of sample A-SFS required more than 9 h of alkali treatment at the hydrothermal condition.

3.4.2. Optimisation of reaction temperature

Additional experiments were conducted to optimise the reaction temperature in which the reaction was carried out at various temperatures of 150, 175, 200, 225, and 250 °C keeping a constant interval of 3 h. The depolymerisation observed below 200 °C resulted in poor yield of sodium silicate i.e., 23.7% (150 °C) and 58.9% (175 °C). About 97.6% and 97.9% yield was observed at higher temperatures of 225 °C and 250 °C respectively (Fig. 5(b)). Therefore, the optimised reaction time and reaction temperature were determined to be 3 h and 225 °C, respectively. The morphologies of residues obtained at different reaction temperatures were analysed, as presented in Fig. 7. It is interesting to note that the silicate network depolymerisation was not effective at temperatures below 200 °C. This occurred because the depolymerisation of angular to hexagonal rod structures was observed only after 3 h reaction at 200 °C, whereas no such hexagonal rod morphology was observed for samples reacted at 150 °C and 175 °C. The samples subjected to reaction at 225 °C and 250 °C showed both hexagonal rod and granular morphologies. This is due to effective etching of the quartz network by the alkali at 225 °C, which led to the depolymerisation of A-SFS (quartz) into sodium silicate.

The XRD patterns of the residues collected at all temperatures also support the FE-SEM observations. No significant impact was observed in depolymerisation, which was evident from the existence of $2\theta = 26.7°$ corresponding to the (101) plane of quartz silica below 225 °C (Fig. 7). The residue obtained from sample subjected to 250 °C showed disintegration of the major peak at $2\theta = 26.7°$. New peaks formed at $2\theta = 26.4°$, $26.5°$, and $26.7°$ confirms the occurrence of disintegration of quartz silicate at 250 °C owing to the action of alkaline depolymerisation (Fig. 7).

3.4.3. Reactivity of alkalis

In order to investigate the role of NaOH, experiments were performed by replacing 2 M NaOH with 2 M KOH at 200 °C at different intervals. The reaction carried out at 3, 6, 9, and 12 h, yields potassium silicates in 48, 76.1, 80.5, and 89.8%, respectively (Fig. S4). The observed quantities of K_2SiO_3 were comparatively lower than those of the yield obtained with NaOH. Gratz et al. (1990) studied the dissolution of quartz in aqueous alkali (LiOH, NaOH, KOH, RbOH, and CsOH) over various temperatures ranges of 106 °C−236 °C and found that KOH had a strong impact on the quartz solubility. But, the present condition may be explained such that NaOH played a more effective role in the depolymerisation of
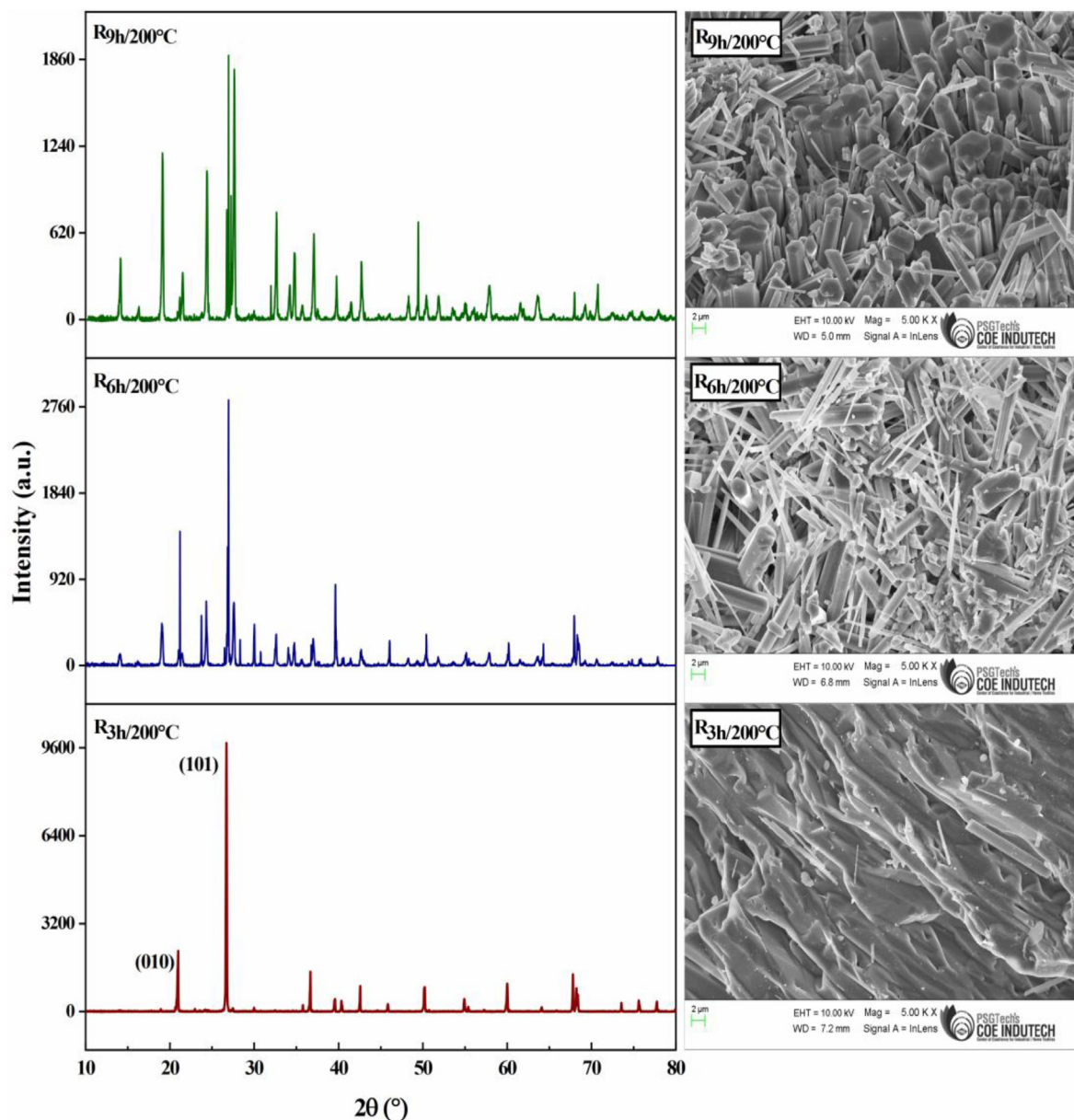
Fig. 6. XRD patterns of residues collected after different periods of subjection at 200 °C; the inset shows the corresponding SEM images.

A-SFS than that of KOH owing to the more efficient intercalation of Na^+ ions than K^+ ions (Crundwell, 2017). Comparatively, Na^+ forms an effective hydration shell over the silica cores through its strongest interaction than the K^+ ion (Crundwell, 2017).

Raza et al. (2018) reported on the alkali dissolution of olivine, a natural silicate rock, in an alkaline medium in which, the maximum dissolution of silicate solution was observed with equal concentrations of NaOH and KOH at high contents of 7 g NaOH:7 g KOH against 10 g of olivine. This phenomenon suggests that temperature and pressure existing in the pressure vessel are more important than the alkali concentration for achieving the maximum yield. Thus, in the present study, 97.6% yield was obtained with 2 mol equivalents of NaOH in comparison with A-SFS under optimal temperature (225 °C) and time (3 h).

3.5. Environmental and economic aspects

The present work describes the remedial utilisation of SFS in an environmentally friendly manner. In particular, this work highlights the possibility of utilising SFS as a precursor in the synthesis of sodium silicate, which in turn can be used in various industries. Moreover, this study serves as a guide for constructive utilisation of SFS as an alternative to the environmentally hazardous disposal method of traditional deposition in landfill. The parallel production of sodium silicate in foundry industries using SFS after preliminary treatment can have an economic impact because the produced sodium silicate has significant industrial importance and good global market value (Weldes and Lange, 1969). Further, the proposed approach is in accordance with recommendations of government environment policies such as zero discharge. This method opens a new gateway under the "Make in India" paradigm to provide socio-economic and environmental benefits for the country. It should also be noted that the rapid depletion of non-renewable natural minerals can be mitigated through this minimalistic, environmentally friendly approach (Kamseu et al., 2017).
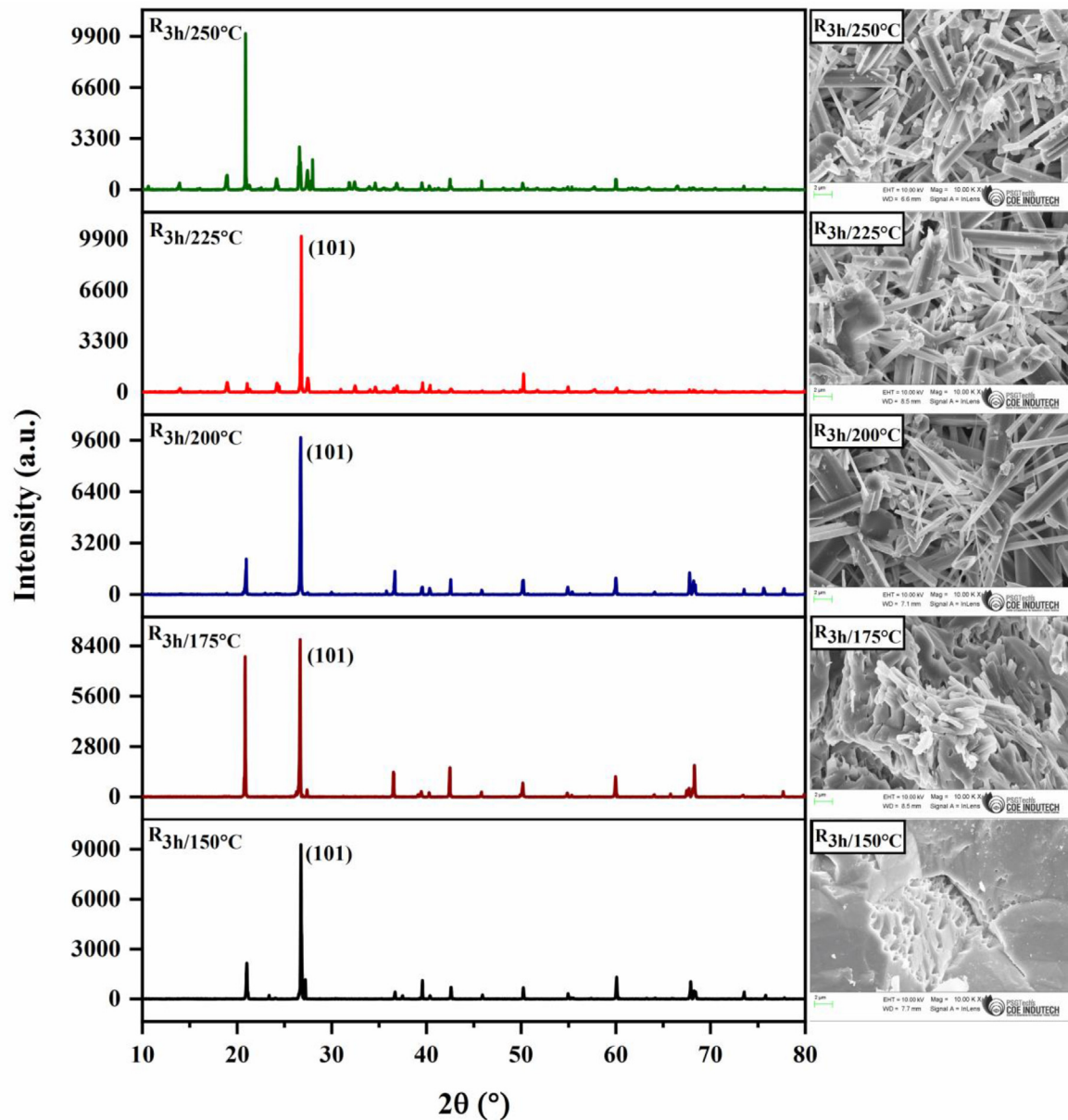
Fig. 7. XRD patterns of A-SFS treated at different temperatures for 3 h; the inset shows the corresponding SEM images.

4. Conclusion

Industrial foundry waste collected from local sources has been successfully synthesized into alkali silicate. The SFS was subjected to calcination followed by acid bleaching treatment, which resulted in low-quartz silica of high purity. The results of XRD and FE-SEM analysis suggest that the treatment processes were effective in removing carbon, clay, and metal impurities. The obtained quartz was converted into sodium silicate using NaOH through the hydrothermal process. The reaction conditions were optimised using different alkali (NaOH and KOH), time intervals, and temperatures. The results of residual analysis using ^{29}Si NMR, XRD, and FE-SEM after the course of different reaction conditions suggest that the possible route of preparation was achieved by the depolymerisation mechanism. The optimised experimental conditions were observed to be 225 °C and 3 h for resulting maximum yield of 97.6%. Thus, the present work demonstrates that SFS can be effectively transformed into a viable commercial alkali silicate product.

Author contribution

M. I. Abdul Aleem: Conceptualization, Validation, Resources, Funding acquisition

K. Kavikumaran: Investigation, Visualization

P. Prabunathan: Methodology, Writing - Original Draft

A. Hariharan: Visualization, Data Curation, Formal analysis

M. Alagar: Supervision, Project administration, Writing - Review & Editing

Declaration of competing interest

The authors declare that they have no known competing financial interests or personal relationships that could have appeared to influence the work reported in this paper.

for their instrumental support and PSG & Sons' charities, Coimbatore, Tamilnadu, India for their financial support.

Appendix A. Supplementary data

Supplementary data related to this article can be found at https://doi.org/10.1016/j.jclepro.2020.121689.

References

Alam, Q., Hendrix, Y., Thijs, L., Lazaro, A., Schollbach, K., Brouwers, H.J.H., 2019. Novel low temperature synthesis of sodium silicate and ordered mesoporous silica from incineration bottom ash. J. Clean. Prod. 211, 874−883.

Allu, A.R., Gaddam, A., Ganisetti, S., Balaji, S., Siegel, R., Mather, G.C., Fabian, M., Pascual, M.J., Ditaranto, N., Milius, W., Senker, J., Agarkov, D.A., Kharton, V.V., Ferreira, J.M.F., 2018. Structure and crystallization of alkaline-earth alumino-silicate glasses: prevention of the alumina-avoidance principle. J. Phys. Chem. B 122, 4737−4747.

Alonso-Santurde, R., Andrés, A., Viguri, J.R., Raimondo, M., Guarini, G., Zanelli, C., Dondi, M., 2011. Technological behaviour and recycling potential of spent foundry sands in clay bricks. J. Environ. Manag. 92, 994−1002.

Anbalagan, G., Prabakaran, A.R., Gunasekaran, S., 2010. Spectroscopic characterization of indian standard sand. J. Appl. Spectrosc. 77, 86−94.

Anderson, G.M., Burnham, C.W., 1965. The solubility of quartz in super-critical water. Am. J. Sci. 263, 494−511.

Arulrajah, A., Yaghoubi, E., Imteaz, M., Horpibulsuk, S., 2017. Recycled waste foundry sand as a sustainable subgrade fill and pipe-bedding construction material: engineering and environmental evaluation. Sustain. Cities Soc. 28, 343−349.

Bakis, R., Koyuncu, H., Demirbas, A., 2006. An investigation of waste foundry sand in asphalt concrete mixtures. Waste Manag. Res. 24, 269−274.

Balbay, S., 2019. Recycling of waste foundry sands by chemical washing method. China Foundry 16, 141−146.

Basar, H.M., DeveciAksoy, N., 2012. The effect of waste foundry sand (WFS) as partial replacement of sand on the mechanical, leaching and micro-structural characteristics of ready-mixed concrete. Construct. Build. Mater. 35, 508−515.

Bass, J.L., Turner, G.L., 2002. Anion distributions in sodium silicate solutions. Characterization by 29 SI NMR and infrared spectroscopies, and vapor phase osmometry. J. Phys. Chem. B 101, 10638−10644.

Bhat, S.T., Lovell, C.W., 1997. Flowable fill using waste foundry sand: a substitute for compacted or stabilized soil. In: Wasemiller, M.A., Hoddinott, K.B. (Eds.), Testing Soil Mixed with Waste or Recycled Materials. ASTM International, West Conshohocken, PA, pp. 26−41.

Crundwell, F.K., 2017. On the mechanism of the dissolution of quartz and silica in aqueous solutions. ACS Omega 2, 1116−1127.

de Matos, P.R., Marcon, M.F., Schankoski, R.A., Prudêncio, L.R., 2019. Novel applications of waste foundry sand in conventional and dry-mix concretes. J. Environ. Manag. 244, 294−303.

de Matos, P.R., Pilar, R., Bromerchenkel, L.H., Schankoski, R.A., Gleize, P.J.P., de Brito, J., 2020. Self-compacting mortars produced with fine fraction of calcined waste foundry sand (WFS) as alternative filler: fresh-state, hydration and hardened-state properties. J. Clean. Prod. 252, 119871.

Díaz Pace, D.M., Miguel, R.E., Di Rocco, H.O., AnabitarteGarcía, F., Pardini, L., Legnaioli, S., Lorenzetti, G., Palleschi, V., 2017. Quantitative analysis of metals in waste foundry sands by calibration free-laser induced breakdown spectroscopy. Spectrochim. Acta Part B At. Spectrosc. 131, 58−65.

Friedman, I.I., 1948. The solubility of quartz in sodium carbonate solutions at high temperature. J. Am. Chem. Soc. 70, 2649−2650.

Gratz, A.J., Bird, P., Quiro, G.B., 1990. Dissolution of quartz in aqueous basic solution, 106-236°C: surface kinetics of "perfect" crystallographic faces. Geochem. Cosmochim. Acta 54, 2911−2922.

Guney, Y., Aydilek, A.H., Demirkan, M.M., 2006. Geoenvironmentalbehavior of foundry sand amended mixtures for highway subbases. Waste Manag. 26, 932−945.

Kamseu, E., Beleuk à Moungam, L.M., Cannio, M., Billong, N., Chaysuwan, D., Melo, U.C., Leonelli, C., 2017. Substitution of sodium silicate with rice husk ash-NaOH solution in metakaolin based geopolymer cement concerning reduction in global warming. J. Clean. Prod. 142, 3050−3060.

Khatib, J.M., Ellis, D.J., 2001. Mechanical properties of concrete containing foundry sand. ACI Spec. Publ. 200, 733−748.

Khouchaf, L., Hamoudi, A., Cordier, P., 2009. Evidence of depolymerisation of amorphous silica at medium- and short-range order: XANES, NMR and CP-SEM contributions. J. Hazard Mater. 168, 1188−1191.

Laudise, R.A., Ballman, A.A., 1961. The solubility of quartz under hydrothermal conditions. J. Phys. Chem. 65, 1396−1400.

Mastella, M.A., Gislon, E.S., Pelisser, F., Ricken, C., Silva, L., da Angioletto, E., Montedo, O.R.K., 2014. Mechanical and toxicological evaluation of concrete artifacts containing waste foundry sand. Waste Manag. 34, 1495−1500.

Moravetski, V., Hill, J.-R., Eichler, U., Cheetham, A.K., Sauer, J., 2002. 29 Si NMR chemical shifts of silicate species: ab initio study of environment and structure effects. J. Am. Chem. Soc. 118, 13015−13020.

Partridge, B.K., Fox, P.J., Alleman, J.E., Mast, D.G., 1999. Field demonstration of highway embankment construction using waste foundry sand. Transport. Res. Rec. 1670, 98−105.

Pfeiffer, T., Sander, S.A.H., Enke, D., Roggendorf, H., 2019. Hydrothermal dissolution of low-quartz in sodium hydroxide lyes: kinetics and equilibrium. Chem. Ing. Tech. 91, 92−101.

Raza, N., Raza, W., Madeddu, S., Agbe, H., Kumar, R.V., Kim, K.H., 2018. Synthesis and characterization of amorphous precipitated silica from alkaline dissolution of olivine. RSC Adv. 8, 32651−32658.

Siddique, R., Singh, G., Singh, M., 2018. Recycle option for metallurgical by-product (Spent Foundry Sand) in green concrete for sustainable construction. J. Clean. Prod. 172, 1111−1120.

Siddiquea, R., Kaur, G., Rajor, A., 2010. Waste foundry sand and its leachate characteristics. Resour. Conserv. Recycl. 54, 1027−1036.

Smith, K.A., Kirkpatrick, R.J., Oldfield, E., Henderson, D.M., 1983. High-resolution silicon-29 nuclear magnetic resonance spectroscopic study of rock-forming silicates. Am. Mineral. 68, 1206−1215.

Souza, C. dos S., Antunes, M.L.P., Valentina, L.V.O.D., Rangel, E.C., da Cruz, N.C., 2019. Use of waste foundry sand (WFS) to produce protective coatings on aluminum alloy by plasma electrolytic oxidation. J. Clean. Prod. 222, 584−592.

Tarek, A., H, B.C., B, E.T., 2000. Foundry green sands as hydraulic barriers: laboratory study. J. Geotech. Geoenviron. Eng. 126, 1174−1183.

Torres, A., Bartlett, L., Pilgrim, C., 2017. Effect of foundry waste on the mechanical properties of Portland Cement Concrete. Construct. Build. Mater. 135, 674−681.

US DOT, 1998. User Guidelines for Waste and By-Product Materials in Pavement Construction. https://www.fhwa.dot.gov/publications/research/infrastructure/structures/97148/fs1.cfm. (Accessed 28 March 2020).

Van Dokkum, H.P., Hulskotte, J.H.J., Kramer, K.J.M., Wilmot, J., 2004. Emission, fate and effects of soluble silicates (Waterglass) in the aquatic environment. Environ. Sci. Technol. 38, 515−521.

Weldes, H.H., Lange, K.R., 1969. Properties of soluble silicates. Ind. Eng. Chem. 61, 29−44.

Wijnen, P.W.J.G., Beelen, T.P.M., de Haan, J.W., Rummens, C.P.J., van de Ven, L.J.M., van Santen, R.A., 1989. Silica gel dissolution in aqueous alkali metal hydroxides studied by ^{29}Si NMR. J. Non-Cryst. Solids 109, 85−94.

Xiang, R., Li, Y., Li, S., Xue, Z., He, Z., Ouyang, S., Xu, N., 2019. The potential usage of waste foundry sand from investment casting in refractory industry. J. Clean. Prod. 211, 1322−1327.

Zion Market Research, 2019. Global sodium silicate market will reach USD 11.67 X 10^9 by 2024. https://www.globenewswire.com/news-release/2019/01/10/1686127/0/en/Global-Sodium-Silicate-Market-Will-Reach-USD-11-67-Billion-By-2024-Zion-Market-Research.html (last accessed: 28/03/2020).